CrossMark

The influence of loading rates on hardening effects in elasto/viscoplastic strain-hardening materials

Fabio De Angelis¹ (iD) · **Donato Cancellara¹** ·
Luigi Grassia² · Alberto D'Amore²

Abstract In this paper the influence of increasing loading rates on hardening effects is analyzed for rate-dependent elastoplastic materials. The effects of different loading rates on hardening rules are discussed with regard to the constitutive behavior of strain-hardening materials in elasto/viscoplasticity. A suitable procedure for the numerical simulation of rate-sensitive material behavior is illustrated. A comparative analysis is presented on constitutive relations in strain-hardening plasticity without rate effects and with rate effects in order to show the different role played by hardening rules in the rate-sensitivity analysis of elasto/viscoplastic strain-hardening materials. By reporting suitable numerical simulations for the adopted constitutive relations it is shown that when the rate of application of the loading is increased the influence of hardening has a different effect in the mechanical behavior of structures. Computational results and applications are finally illustrated in order to show numerically the different role played by hardening on the plastic strains when the loading rates are incremented for elasto/viscoplastic strain-hardening materials and structures.

Keywords Hardening rules · Elasto/viscoplasticity · Rate-sensitive materials ·
Time-dependent material behavior · Finite Element Method

1 Introduction

Rate dependence of constitutive behavior of strain-hardening materials is a typical time-dependent phenomenon. In fact, the rate-dependent plastic behavior of materials and structures is of considerable scientific interest in most common industrial applications; see, for instance, the assessment of safety and reliability of mechanical and aeronautical structures,

✉ F. De Angelis
fabio.deangelis@unina.it

1   Department of Structures for Engineering and Architecture, University of Naples Federico II,
    via Claudio 21, 80125 Naples, NA, Italy

2   Department of Industrial and Information Engineering, University of Campania "Luigi Vanvitelli",
    via Roma 19, 81031 Aversa, CE, Italy

the mechanical behavior of beams plates and shells, the calculation of piping, pressure vessels and jet engine turbine blades.

In the last two decades rate-dependent plasticity has achieved a significant progress, both in the definition of the appropriate theoretical framework of the phenomenon and in the computational treatment of the model. Computational algorithms for the simulation of nonlinear kinematic hardening rules have been presented by Artioli et al. (2007). Computational issues and numerical applications in rate-dependent plasticity with hardening have been discussed by DeAngelis (2013). An efficient return mapping algorithm for elastoplasticity with nonlinear hardening and an exact closed form solution of the local constitutive problem has been proposed by DeAngelis and Taylor (2015) and DeAngelis and Taylor (2016). Constitutive modeling of ductile materials for static and dynamic applications have been investigated, among others, by Abed (2010). Ductile failure behavior of materials has been analyzed under different loading conditions by Autenrieth et al. (2009). Experimental results and analyses regarding the behavior of ductile metals under different environmental conditions have been studied by Brnic et al. (2011). An experimental-numerical approach has been adopted by Pina et al. (2014) to simulate the mechanical response of ductile metals. The effects of cyclic loadings and fatigue of materials have been investigated, among others, by D'Amore et al. (2013), Farrahi et al. (2014) and D'Amore and Grassia (2016). For a nonlocal approach in rate plasticity, see, e.g., Marotti de Sciarra (2004) and Marotti de Sciarra (2008). For a comprehensive account on the computational simulation of strain-hardening elasto/viscoplasticity see, among others, Simo and Hughes (1998), Simo (1998), and Zienkiewicz et al. (2013).

In the present paper we refer to evolutive processes in rate-sensitive strain-hardening materials and structures. A suitable algorithmic procedure is adopted, which is based on an implicit backward difference method. The adopted numerical procedure is consistent with the variational formulation of rate-dependent plasticity and viscoplasticity problems, see, e.g., DeAngelis (2000). An appropriate solution strategy is adopted, which is suitable to be specialized to different constitutive models and arbitrary yield criteria. Numerical algorithms are considered for rate-dependent plasticity models which account for rate-dependent loading effects in the mechanical response of strain-hardening materials and structures. A suitable implicit backward difference method is applied and an appropriate numerical solution scheme is illustrated for elasto/viscoplasticity which accounts for rate-dependent loadings.

It is emphasized, however, that the present research work does not specifically address investigations on the efficiency of different algorithmic aspects of solids loaded in the plastic range. In fact, in this regard the interested reader may refer to, among others, DeAngelis and Cancellara (2017). Conversely, in the present paper numerical results are analyzed in order to investigate the influence that hardening rules have on constitutive relations in the mechanical response of rate-dependent elastoplastic strain-hardening materials when the loadings are applied with increasing prescribed loading rates. A comparative analysis is discussed and remarks are reported on the differentiated effects that hardening rules have on the mechanical behavior of rate-sensitive elastoplastic materials depending on the rate of application of the loadings.

In the analysis, considerations are reported on the effects that hardening rules have on the mechanical behavior of rate-dependent elastoplastic strain-hardening materials and structures. Some remarks are presented on the different role played by hardening in the rate-sensitivity analysis of material behavior. The influence of different loading rates is discussed with reference to the simulation of the rate-dependent elastoplastic strain-hardening behavior of materials.

An investigation is presented on the effects of hardening in the mechanical response of the constitutive relations in strain-hardening elasto/viscoplasticity with and without rate

effects so that the different role played by hardening is emphasized in the rate-sensitive mechanical behavior of materials and structures.

In the paper for the considered constitutive relations the illustrated computational simulations are compared with experimental results reported in the literature. Computational results are finally described in order to illustrate numerically the effectiveness of the reported considerations for the adopted constitutive relations. Accordingly, the different effects that hardening rules have on the maximum plastic strains and on the inelastic material behavior are emphasized for elasto/viscoplastic strain-hardening materials and structures in which the loadings are applied with different and increased loading rates.

2 The continuum problem

For the body $\mathcal{B}$ we define the reference configuration $\Omega \subset \mathfrak{R}^n$, $1 \leq n \leq 3$, and indicate the particles by their position vector $\mathbf{x} \in \Omega$ relative to a Cartesian coordinate system. Let $\mathcal{T} \subset \mathfrak{R}_+$ be the time interval of interest and V be the space of displacements, D the strain space and S the dual stress space. We indicate with $\mathbf{u} : \Omega \times \mathcal{T} \to V$ the displacement vector and with $\boldsymbol{\sigma} : \Omega \times \mathcal{T} \to S$ the stress tensor. The compatible strain tensor is defined by $\boldsymbol{\varepsilon}(\mathbf{u}) = \nabla^s(\mathbf{u}) : \Omega \times \mathcal{T} \to D$, where ∇^s is the symmetric part of the gradient.

We assume the framework of a small strain theory with quasi-static deformations, i.e., without inertia effects. Furthermore, we refer to the class of materials often denoted in the literature as *rate-sensitive* materials, see, e.g., Skrzypek and Hetnarski (1993). Accordingly, viscous effects are assumed to exhibit beyond the elastic range, see also Naghdi and Murch (1963) and Perzyna (1966). Consequently, we will indicate with $\boldsymbol{\varepsilon}^{\mathrm{vp}}$ the viscoplastic strain, where combined viscous and plastic effects are represented and the strain difference $\boldsymbol{\varepsilon}^e = \boldsymbol{\varepsilon} - \boldsymbol{\varepsilon}^{\mathrm{vp}}$ is identified as the elastic strain. For a comprehensive analysis, see, e.g., Duvaut and Lions (1992) and Lemaitre and Chaboche (1990).

For modeling hardening behavior we introduce a dual pair of kinematic $\boldsymbol{\alpha} = (\boldsymbol{\alpha}_{\mathrm{kin}}, \alpha_{\mathrm{iso}}) \in X \times \mathfrak{R}$ and static $\boldsymbol{\chi} = (\boldsymbol{\chi}_{\mathrm{kin}}, \chi_{\mathrm{iso}}) \in X' \times \mathfrak{R}$ internal variables, where $\alpha_{\mathrm{iso}} \in \mathfrak{R}$ and $\chi_{\mathrm{iso}} \in \mathfrak{R}$ model isotropic hardening and $\boldsymbol{\alpha}_{\mathrm{kin}} \in X$ and $\boldsymbol{\chi}_{\mathrm{kin}} \in X'$ model kinematic hardening, with X and X' representing dual spaces. Static and kinematic internal variables are related by the expression $\boldsymbol{\chi} = \mathbf{H}\boldsymbol{\alpha}$ where $\mathbf{H} = \mathrm{diag}[\mathbf{H}_{\mathrm{kin}}, H_{\mathrm{iso}}]$ is the hardening matrix.

We introduce the elastic domain $\mathcal{E}$ defined as

$$\mathcal{E} \stackrel{\mathrm{def}}{=} \left\{ (\boldsymbol{\sigma}, \boldsymbol{\chi}_{\mathrm{kin}}, \chi_{\mathrm{iso}}) \in S \times X' \times \mathfrak{R} : f(\boldsymbol{\sigma}, \boldsymbol{\chi}_{\mathrm{kin}}, \chi_{\mathrm{iso}}) \leq 0 \right\}, \tag{1}$$

where $f(\boldsymbol{\sigma}, \boldsymbol{\chi}_{\mathrm{kin}}, \chi_{\mathrm{iso}})$ is a convex yield function. The yield function is assumed to be expressed in the form

$$f(\boldsymbol{\sigma}, \boldsymbol{\chi}_{\mathrm{kin}}, \chi_{\mathrm{iso}}) = F(\boldsymbol{\sigma} - \boldsymbol{\chi}_{\mathrm{kin}}) - \kappa(\chi_{\mathrm{iso}}), \tag{2}$$

where $\kappa(\chi_{\mathrm{iso}})$ is a material hardening parameter.

We also introduce the elastic energy $\mathcal{W} : D \to \mathfrak{R}$ and the complementary elastic energy $\mathcal{W}^* : S \to \mathfrak{R}$, which are expressed for linear elasticity in the quadratic forms

$$\mathcal{W}(\boldsymbol{\varepsilon}^e) = \frac{1}{2}\langle \mathbf{C}\boldsymbol{\varepsilon}^e, \boldsymbol{\varepsilon}^e \rangle, \qquad \mathcal{W}^*(\boldsymbol{\sigma}) = \frac{1}{2}\langle \boldsymbol{\sigma}, \mathbf{C}^{-1}\boldsymbol{\sigma} \rangle. \tag{3}$$

Herein $\mathbf{C}$ denotes the elastic stiffness and the symbol $\langle \bullet, \bullet \rangle$ represents the inner product in the dual spaces with the meaning of $\langle \bullet, \bullet \rangle \stackrel{\mathrm{def}}{=} \int_{\Omega} \bullet \cdot \bullet \, \mathrm{d}\Omega$, where $\cdot$ denotes the simple (double) index saturation operation between vectors (tensors).

3 Evolutive problem in rate-dependent plasticity

In the sequel we develop the evolutive rate plastic problem with hardening within the framework provided by Halphen and Nguyen (1975) in which strains and kinematic internal variables, as well as the corresponding dual static variables, are collected in suitably defined generalized variables

$$\mathbf{E} = (\boldsymbol{\varepsilon}, \mathbf{o}), \qquad \mathbf{E}^e = (\boldsymbol{\varepsilon}^e, \boldsymbol{\alpha}), \qquad \mathbf{E}^{\mathrm{vp}} = (\boldsymbol{\varepsilon}^{\mathrm{vp}}, -\boldsymbol{\alpha}), \qquad \boldsymbol{\Sigma} = (\boldsymbol{\sigma}, \boldsymbol{\chi}). \tag{4}$$

The generalized kinematic and static variables are defined respectively in the product spaces $\tilde{\boldsymbol{D}} = \boldsymbol{D} \times \boldsymbol{X} \times \Re$ and $\tilde{\boldsymbol{S}} = \boldsymbol{S} \times \boldsymbol{X}' \times \Re$.

Given a generalized viscoplastic strain $\dot{\mathbf{E}}^{\mathrm{vp}}$, among all possible generalized stresses $\boldsymbol{\Gamma} = (\boldsymbol{\tau}, \mathbf{q}) \in \tilde{\boldsymbol{S}}$, the actual generalized stress $\boldsymbol{\Sigma} = (\boldsymbol{\sigma}, \boldsymbol{\chi})$ satisfies the principle of maximum dissipation, see, e.g., Hill (1950),

$$D^{\mathrm{vp}}(\dot{\mathbf{E}}^{\mathrm{vp}}) = \sup_{\boldsymbol{\Gamma} \in \tilde{\boldsymbol{S}}} \{\langle \boldsymbol{\Gamma}, \dot{\mathbf{E}}^{\mathrm{vp}} \rangle - \Pi^*(\boldsymbol{\Gamma})\}, \tag{5}$$

where $\Pi^*(\boldsymbol{\Gamma})$ represents a viscoplastic convex potential.

The optimality conditions (5) can be expressed in terms of the viscoplastic Lagrangian

$$\mathcal{L}^{\mathrm{vp}}(\boldsymbol{\Gamma}) \stackrel{\mathrm{def}}{=} -\langle \boldsymbol{\Gamma}, \dot{\mathbf{E}}^{\mathrm{vp}} \rangle + \Pi^*(\boldsymbol{\Gamma}). \tag{6}$$

Accordingly, among all possible generalized stresses $\boldsymbol{\Gamma} = (\boldsymbol{\tau}, \mathbf{q}) \in \tilde{\boldsymbol{S}}$, the optimal generalized stress $\boldsymbol{\Sigma} = (\boldsymbol{\sigma}, \boldsymbol{\chi})$ is obtained by enforcing the stationarity condition for $\mathcal{L}^{\mathrm{vp}}(\boldsymbol{\Gamma})$

$$\left[\partial \mathcal{L}^{\mathrm{vp}}(\boldsymbol{\Gamma}) \right]_{(\boldsymbol{\Sigma})} = 0 \quad \Longleftrightarrow \quad \dot{\mathbf{E}}^{\mathrm{vp}} = \partial \Pi^*(\boldsymbol{\Sigma}), \tag{7}$$

which expresses in generalized variables the flow law of the viscoplastic strain and the evolutive laws of the kinematic internal variables. In order to take into account the multivaluedness of the viscoplastic evolutive problem, the above equation can be expressed in subdifferential form, see, e.g., DeAngelis (2000).

The flow rule $(7)_2$ can be formulated in the inverse equivalent form

$$\boldsymbol{\Sigma} = \partial D^{\mathrm{vp}}(\dot{\mathbf{E}}^{\mathrm{vp}}), \tag{8}$$

or equivalently in the Fenchel's form, see, e.g., Hiriart-Urruty and Lemarechal (1993),

$$\Pi^*(\boldsymbol{\Sigma}) + D^{\mathrm{vp}}(\dot{\mathbf{E}}^{\mathrm{vp}}) = \langle \boldsymbol{\Sigma}, \dot{\mathbf{E}}^{\mathrm{vp}} \rangle. \tag{9}$$

By resorting to the penalty regularization procedure, see, e.g., Yosida (1980), the constrained optimization problem related to the plastic model is formulated as an unconstrained problem. Let us introduce the penalty function $g^+(x)$ of the constraint $f(\boldsymbol{\Gamma})$. A penalty function is required to satisfy the following conditions: $g^+(x)$ is continuous in $[0, \infty)$, $g^+(x) \geq 0$ and convex in $[0, \infty)$, $g^+(x) = 0$ if and only if $x \leq 0$. Under such assumptions, the regularized form of the Lagrangian (6) is expressed by

$$\mathcal{L}_\eta^{\mathrm{vp}}(\boldsymbol{\Gamma}) \stackrel{\mathrm{def}}{=} -\langle \boldsymbol{\Gamma}, \dot{\mathbf{E}}^{\mathrm{vp}} \rangle + \frac{1}{\eta} g^+(f(\boldsymbol{\Gamma})), \tag{10}$$

where $\eta > 0$ is the penalty parameter with the significance of a viscosity coefficient.

Accordingly, the regularized form of the viscoplastic dissipation is formulated by

$$D_\eta^{\mathrm{vp}}\big(\dot{\mathbf{E}}^{\mathrm{vp}}\big) = \sup_{\boldsymbol{\Gamma} \in \tilde{\mathcal{S}}} \left\{ \langle \boldsymbol{\Gamma}, \dot{\mathbf{E}}^{\mathrm{vp}} \rangle - \frac{1}{\eta} g^+\big(f(\boldsymbol{\Gamma}) \big) \right\}. \tag{11}$$

The solution $\boldsymbol{\Sigma}_\eta$ of the regularized problem tends to the solution $\boldsymbol{\Sigma}$ of the constrained plastic problem for $\eta \to 0^+$, see, e.g., Luenberger (1973). The viscoplastic constitutive problem is therefore regarded in the literature as a *penalty regularization* of the plastic constitutive problem.

Different formulations of the viscoplastic constitutive relations are obtained by suitably specializing the penalty function. The penalty function g^+ can be suitably expressed by

$$g^+(x) \overset{\text{def}}{=} \begin{cases} \frac{1}{2}x^2 & \text{for } x \geq 0, \\ 0 & \text{for } x < 0, \end{cases} \tag{12}$$

the derivative is expressed by $\frac{dg^+(x)}{dx} = \langle x \rangle$, where the MacAuley brackets $\langle \cdot \rangle$ are defined by $\langle x \rangle = (x + |x|)/2$.

For modeling nonlinear viscous effects it is useful to introduce the flow function $\Phi(x)$ such that $\frac{dg^+(x)}{dx} = \langle \Phi(x) \rangle$. By recalling the regularized viscoplastic potential (10), the viscoplastic flow rule (7) supplies

$$\big[\partial \mathcal{L}_\eta^{\mathrm{vp}}(\boldsymbol{\Gamma}) \big]_{(\boldsymbol{\Sigma})} = 0 \quad \Longleftrightarrow \quad \dot{\mathbf{E}}^{\mathrm{vp}} = \frac{1}{\eta} \langle \Phi\big(f(\boldsymbol{\Sigma}) \big) \rangle \partial f(\boldsymbol{\Sigma}), \tag{13}$$

which expresses in generalized variables the evolutive law of the Perzyna viscoplastic constitutive model, see, e.g., Perzyna (1963). For linear viscous effects a standard choice of the flow function is $\Phi(f(\boldsymbol{\Sigma})) = f(\boldsymbol{\Sigma})$. For nonlinear viscous effects, different proposals of the flow function are reported, e.g., by Skrzypek and Hetnarski (1993).

The interpretation of the evolutive problem in viscoplasticity as optimality condition of a convex optimization problem has proven to be useful of providing a complete variational formulation for the viscoplastic structural problem, see, e.g., DeAngelis (2000), and it is well suited for the formulation of variationally consistent numerical algorithms in finite element applications.

4 Discrete formulation and algorithmic procedure

We consider the elastic domain as expressed by a von Mises yield criterion

$$f(\boldsymbol{\sigma}, \boldsymbol{\chi}_{\mathrm{kin}}, \chi_{\mathrm{iso}}) = \| \operatorname{dev} \boldsymbol{\sigma} - \boldsymbol{\chi}_{\mathrm{kin}} \| - \kappa(\chi_{\mathrm{iso}}) = \| \boldsymbol{\eta} \| - \sqrt{\frac{2}{3}}(\sigma_{\mathrm{yo}} + \chi_{\mathrm{iso}}) \leq 0, \tag{14}$$

in which $\operatorname{dev}\boldsymbol{\sigma}$ denotes the stress deviator, $\boldsymbol{\eta} \overset{\text{def}}{=} \operatorname{dev}\boldsymbol{\sigma} - \boldsymbol{\chi}_{\mathrm{kin}}$ is the relative stress, $\kappa(\chi_{\mathrm{iso}}) = \sqrt{\frac{2}{3}}(\sigma_{\mathrm{yo}} + \chi_{\mathrm{iso}})$ is the current radius of the yield surface in the deviatoric plane, and σ_{yo} represents the uniaxial yield stress of the virgin material.

An associative rate-dependent plastic behavior is assumed so that during an increment of plastic strain the yield surface moves in the direction of the exterior normal to the yield

surface at the considered stress point. Accordingly, the evolutive flow law for the constitutive equation in associative rate-dependent plasticity is expressed by

$$\dot{\boldsymbol{\varepsilon}}^{\mathrm{vp}} = \dot{\gamma}^{\mathrm{vp}} \frac{\partial f}{\partial \boldsymbol{\sigma}} = \dot{\gamma}^{\mathrm{vp}} \frac{\partial f}{\partial \boldsymbol{\eta}} = \dot{\gamma}^{\mathrm{vp}} \mathbf{n}, \qquad (15)$$

in which $\dot{\gamma}^{\mathrm{vp}}$ is the viscoplastic multiplier, the second rank tensor $\mathbf{n}$ is given by $\mathbf{n} \stackrel{\text{def}}{=} \frac{\boldsymbol{\eta}}{\|\boldsymbol{\eta}\|}$, and the accumulated equivalent viscoplastic strain rate is expressed by $\dot{\bar{e}}^{\mathrm{vp}} = \sqrt{\frac{2}{3}} \dot{\gamma}^{\mathrm{vp}}$.

A widely adopted hypothesis for strain-hardening assumes the isotropic hardening to produce a change in size of the yield surface in the stress space during continued plastic deformation without change in shape. For linear isotropic hardening the static internal variable related to isotropic hardening is given by $\chi_{\mathrm{iso}} = H_{\mathrm{iso}} \alpha_{\mathrm{iso}}$ and the dual kinematic internal variable α_{iso} is represented by the equivalent viscoplastic strain $\alpha_{\mathrm{iso}} \stackrel{\text{def}}{=} \bar{e}^{\mathrm{vp}} = \int_0^t \sqrt{\frac{2}{3}} \|\dot{\boldsymbol{\varepsilon}}^{\mathrm{vp}}\| \, \mathrm{d}t$.

For nonlinear isotropic hardening it is often assumed

$$\chi_{\mathrm{iso}} = H_{\mathrm{iso}} (\bar{e}^{\mathrm{vp}})^m, \quad \text{or} \quad \chi_{\mathrm{iso}} = \chi_{\mathrm{iso},\infty} \left(1 - e^{-b\,\bar{e}^{\mathrm{vp}}}\right), \qquad (16)$$

where m, $\chi_{\mathrm{iso},\infty}$ and b are material parameters.

A frequently used kinematic hardening rule is the linear kinematic hardening law proposed by Ishlinsky (1954) and Prager (1956). It is postulated that the kinematic hardening is given by a pure translation of the yield surface in the stress space without change in size. The translation of the yield surface is expressed by the back stress. By assuming linear kinematic hardening the back stress rate is represented in the form

$$\dot{\boldsymbol{\beta}} = \frac{2}{3} H_{\mathrm{kin}} \dot{\boldsymbol{\varepsilon}}^{\mathrm{vp}}, \qquad (17)$$

where it has been assumed $\mathbf{H}_{\mathrm{kin}} = \frac{2}{3} H_{\mathrm{kin}} \mathbf{I}$. The static internal variable related to kinematic hardening is assumed to be the back stress $\chi_{\mathrm{kin}} \stackrel{\text{def}}{=} \boldsymbol{\beta}$, and the dual kinematic internal variable α_{kin} is represented by the viscoplastic strain rate $\dot{\boldsymbol{\varepsilon}}^{\mathrm{vp}}$.

Under the assumption of a nonlinear kinematic hardening behavior, the model proposed by Armstrong and Frederick (1966) is often adopted in the literature, which is expressed by

$$\dot{\boldsymbol{\beta}} = \frac{2}{3} H_{\mathrm{kin}} \dot{\boldsymbol{\varepsilon}}^{\mathrm{vp}} - H_{\mathrm{nl}} \dot{\bar{e}}^{\mathrm{vp}} \boldsymbol{\beta}, \qquad (18)$$

where H_{nl} is a dimensionless material-dependent parameter which is null in case of linear kinematic hardening. A better approximation of nonlinear kinematic hardening behavior consists in adding several components of the back stress with different recall constants (Chaboche 2008):

$$\boldsymbol{\beta} = \sum_{i=1}^{M} \boldsymbol{\beta}_i, \qquad \dot{\boldsymbol{\beta}}_i = \frac{2}{3} H_{\mathrm{kin},i} \dot{\boldsymbol{\varepsilon}}^{\mathrm{vp}} - H_{\mathrm{nl},i} \dot{\bar{e}}^{\mathrm{vp}} \boldsymbol{\beta}_i. \qquad (19)$$

For a comparative analysis of linear and nonlinear kinematic hardening rules for metals and alloys, see, e.g., DeAngelis (2012).

We consider the time interval $\mathcal{T} \subset \Re_+$ specified as $[0, T]$. According to a strain-driven formulation, at a generic time $t_n \in [0, T]$ the total and viscoplastic strain fields and the internal variables are assumed to be known.

At time $t_n \in [0, T]$ a prescribed increment of the displacement field $\Delta\mathbf{u}$ is assigned, that is, a corresponding increment of the strain field $\Delta\boldsymbol{\varepsilon} = \nabla^s(\Delta\mathbf{u})$, which corresponds to assigning the total strain at time $t_{n+1} \in [0, T]$ set equal to $\boldsymbol{\varepsilon}_{n+1} = \boldsymbol{\varepsilon}_n + \nabla^s(\Delta\mathbf{u})$. The algorithmic scheme requires updating all the unknown fields at time $t_{n+1} \in [0, T]$ consistently with the viscoplastic flow rule expressed in generalized variables as

$$\dot{\mathbf{E}}^{\text{vp}} = \frac{1}{\eta}\langle\Phi(f(\boldsymbol{\Sigma}))\rangle\mathrm{d}_{\boldsymbol{\Sigma}}f(\boldsymbol{\Sigma}). \tag{20}$$

In the sequel we make explicit a Perzyna viscoplastic constitutive model with nonlinear viscous effects and, accordingly, the flow rule (20) is expressed in components by

$$\dot{\boldsymbol{\varepsilon}}^{\text{vp}} = \frac{1}{\eta}\langle\Phi(f(\boldsymbol{\sigma}, \boldsymbol{\chi}))\rangle\frac{\boldsymbol{\eta}}{\|\boldsymbol{\eta}\|} = \frac{1}{\eta}\langle\Phi(f(\boldsymbol{\sigma}, \boldsymbol{\chi}))\rangle\mathbf{n},$$

$$\dot{\boldsymbol{\chi}}_{\text{kin}} = \frac{2}{3}H_{\text{kin}}\dot{\boldsymbol{\varepsilon}}^{\text{vp}} = \frac{2}{3}\frac{\langle\Phi(f(\boldsymbol{\sigma}, \boldsymbol{\chi}))\rangle}{\eta}H_{\text{kin}}\frac{\boldsymbol{\eta}}{\|\boldsymbol{\eta}\|} = \frac{2}{3}\frac{\langle\Phi(f(\boldsymbol{\sigma}, \boldsymbol{\chi}))\rangle}{\eta}H_{\text{kin}}\mathbf{n}, \tag{21}$$

$$\dot{\bar{e}}^{\text{vp}} = \sqrt{\frac{2}{3}}\frac{\langle\Phi(f(\boldsymbol{\sigma}, \boldsymbol{\chi}))\rangle}{\eta}.$$

By adopting a fully implicit integration scheme and by recalling that for the back stress $\boldsymbol{\beta} \stackrel{\text{def}}{=} \boldsymbol{\chi}_{\text{kin}}$, we introduce the time step dependent viscoplastic multiplier

$$\gamma_{n+1}^{\text{vp}} = \frac{1}{\eta}\langle\Phi(f(\boldsymbol{\sigma}_{n+1}, \boldsymbol{\beta}_{n+1}, \kappa_{n+1}))\rangle\Delta t, \tag{22}$$

in which $\Delta t = t_{n+1} - t_n$, see, e.g., Simo et al. (1988) and DeAngelis and Cancellara (2017).

Accordingly, the discrete forms of the evolutive equations (21) are specialized into

$$\boldsymbol{\varepsilon}_{n+1}^{\text{vp}} = \boldsymbol{\varepsilon}_n^{\text{vp}} + \gamma_{n+1}^{\text{vp}}\mathbf{n}_{n+1},$$

$$\boldsymbol{\beta}_{n+1} = \boldsymbol{\beta}_n + \frac{2}{3}H_{\text{kin}}\gamma_{n+1}^{\text{vp}}\mathbf{n}_{n+1}, \tag{23}$$

$$\bar{e}_{n+1}^{\text{vp}} = \bar{e}_n^{\text{vp}} + \sqrt{\frac{2}{3}}\gamma_{n+1}^{\text{vp}},$$

and the current radius of the yield surface in the deviatoric plane is expressed by

$$\kappa_{n+1} = \kappa_n + \frac{2}{3}H_{\text{iso}}\gamma_{n+1}^{\text{vp}}. \tag{24}$$

For the numerical scheme it is useful to introduce the strain deviator $\mathbf{v} \stackrel{\text{def}}{=} \mathrm{dev}\,\boldsymbol{\varepsilon}$ and the stress deviator $\mathbf{s} \stackrel{\text{def}}{=} \mathrm{dev}\,\boldsymbol{\sigma}$. An elastic prediction-plastic correction scheme yields the trial values

$$\mathbf{s}_{n+1}^t = 2G(\mathbf{v}_{n+1} - \mathbf{v}_n^{\text{vp}}), \qquad \boldsymbol{\eta}_{n+1}^t = \mathbf{s}_{n+1}^t - \boldsymbol{\beta}_n. \tag{25}$$

Accordingly, at time t_{n+1} the stress deviator and the relative stress are expressed by

$$\mathbf{s}_{n+1} = \mathbf{s}_{n+1}^t - 2G\gamma_{n+1}^{\text{vp}}\mathbf{n}_{n+1}, \qquad \boldsymbol{\eta}_{n+1} = \boldsymbol{\eta}_{n+1}^t - \left(2G + \frac{2}{3}H_{\text{kin}}\right)\gamma_{n+1}^{\text{vp}}\mathbf{n}_{n+1}. \tag{26}$$

The viscoplastic multiplier $\gamma_{n+1}^{\mathrm{vp}}$ and the normal $\mathbf{n}_{n+1}$ can be determined by the algorithmic procedure illustrated by DeAngelis and Cancellara (2017). Consequently, the unknown variables are updated at time t_{n+1} by (23), (24) and (26).

For rate-dependent plasticity problems, the tangent stiffness operator consistent with the algorithmic procedure may be derived within the framework of the generalized standard material model, see DeAngelis and Cancellara (2017). The expression of the consistent tangent operator $\boldsymbol{C}^{\mathrm{vp}}$ for general yield criteria in rate elastoplasticity is thus given by

$$\boldsymbol{C}^{\mathrm{vp}} = \boldsymbol{\Xi}_1 - \frac{\mathbf{N} \otimes \mathbf{N}}{\rho}, \tag{27}$$

where

$$
\begin{aligned}
\mathbf{N} &= \boldsymbol{\Xi}_2 \mathbf{n}, \\
\boldsymbol{\Xi}_1 &= \boldsymbol{C} - \gamma^{\mathrm{vp}} \boldsymbol{C} \mathbf{A} \boldsymbol{C}, \\
\boldsymbol{\Xi}_2 &= \boldsymbol{C} - \gamma^{\mathrm{vp}} \boldsymbol{C} \mathbf{A} (\boldsymbol{C} + \mathbf{H}_{\mathrm{kin}}), \\
\boldsymbol{\Xi}_3 &= (\boldsymbol{C} + \mathbf{H}_{\mathrm{kin}}) - \gamma^{\mathrm{vp}} (\boldsymbol{C} + \mathbf{H}_{\mathrm{kin}}) \mathbf{A} (\boldsymbol{C} + \mathbf{H}_{\mathrm{kin}}), \\
\rho &= \boldsymbol{\Xi}_3 \mathbf{n} \cdot \mathbf{n} + \frac{2}{3} H_{\mathrm{iso}} + \frac{d}{d\gamma^{\mathrm{vp}}} \left[\varPhi^{-1} \left(\frac{\eta}{\Delta t} \gamma^{\mathrm{vp}} \right) \right], \\
\mathbf{A} &= \mathrm{d}_{\sigma\sigma}^2 f \left[\mathbf{I} + \gamma^{\mathrm{vp}} (\boldsymbol{C} + \mathbf{H}_{\mathrm{kin}}) \big(\mathrm{d}_{\sigma\sigma}^2 f \big) \right]^{-1}.
\end{aligned}
\tag{28}
$$

A noteworthy characteristic of such a tangent operator is the applicability to arbitrary yield criteria and to different viscoplastic constitutive models. Different viscoplastic constitutive models may be readily taken into account by suitably specializing the flow function $\varPhi$. Different expressions for the flow function $\varPhi$ for different constitutive models are reported by, among others, Skrzypek and Hetnarski (1993). Another advantage of the above consistent tangent operator is the applicability to arbitrary yield criteria by suitably specializing the relevant yield function f.

With regard to the consistent linearization that is required in plasticity problems, we also note that finite element plasticity formulations without matrix inversions have been investigated by Valoroso and Rosati (2009a) and Valoroso and Rosati (2009b) and for plasticity with nonlinear kinematic hardening by DeAngelis and Taylor (2016).

5 The influence of loading rates on hardening effects for rate-dependent elastoplastic materials and finite element applications

We study the plane strain problem of an infinitely long rectangular strip with a circular hole subject to prescribed edge displacements perpendicular to the axis of the strip. A rate-dependent elastoplastic strain-hardening material behavior is adopted according to the constitutive relations detailed in the previous sections. Details of the geometry the finite element mesh and the loading conditions are illustrated in Fig. 1 (top).

For symmetry conditions only 1/4 of the strip is modeled. The adopted finite element mesh is composed of 325 nodes and 288 elements. In the numerical simulation 4-node bilinear isoparametric quadrilateral elements have been adopted with 2×2 Gaussian quadrature. The mechanical parameters for the material are: elastic modulus $E = 2.1 \times 10^5$ MPa, Poisson's ratio $\nu = 0.3$, yield limit $\sigma_y = 240$ MPa, hardening moduli $H_{\mathrm{iso}} = 2.1 \times 10^3$ MPa,

Fig. 1 Perforated strip. Finite element mesh (*top*). Load vs displacement curves for different values of the loading program parameter τ (*bottom*)
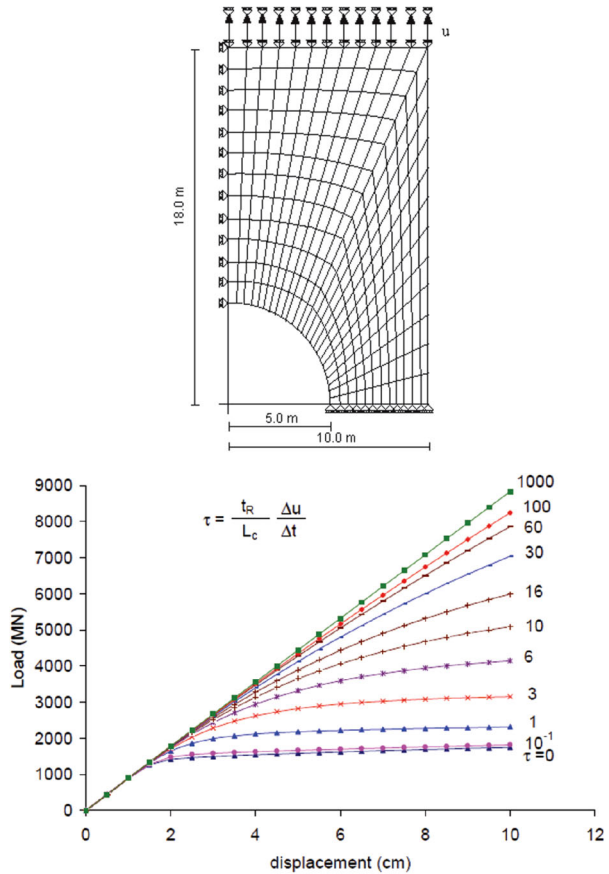
and $H_{\mathrm{kin}} = 6.0 \times 10^2$ MPa. Prescribed upper edge displacements are assigned in single steps Δu up to the final imposed displacement $u_{\mathrm{max}} = 10$ cm.

In the following a dimensionless loading program parameter

$$\tau = \frac{t_R}{L_c} \frac{\Delta u}{\Delta t}$$

is introduced in order to account for the loading rate adopted in the loading process.

The dimensionless loading program parameter τ accounts for the rate $\Delta u/\Delta t$ of the prescribed edge displacement Δu, the intrinsic properties of the material via a relaxation time $t_R = \eta/2G$ and the geometry of the problem by means of a characteristic length of the structural model $L_c = L/c$, where L is the length of the strip and c a dimensionless constant. Herein the dimensionless constant c is introduced in order to decrease the length L to a reduced value $L_c = L/c$. In this numerical example we assumed $c = 2900$. The value of c has been adopted in order to have reasonable values for the loading program parameter τ.

In Fig. 1 (bottom), load versus displacement curves are plotted for different loading program parameters τ. The load is considered to be the sum of the nodal reactions on the bounded upper edge. The rate-independent plastic behavior is recovered for a loading pro-

Fig. 2 Rate-independent plasticity with and without hardening ($\tau = 0$). Maximum equivalent plastic strain exhibited in the loading process vs the applied load (*top*). Maximum equivalent plastic strain exhibited in the loading process vs the prescribed upper edge displacement (*bottom*)
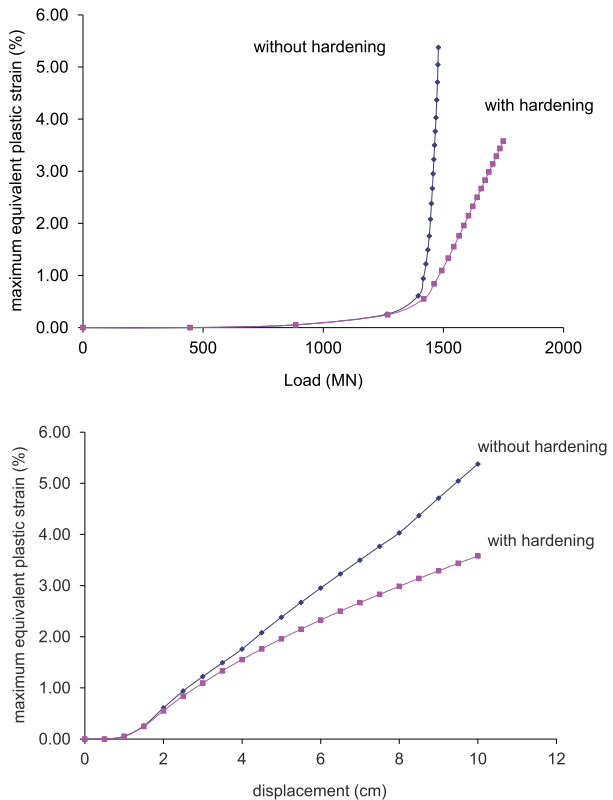
gram parameter $\tau = 0$. The rate-dependent plastic material behavior is recovered for non-null values of the loading program parameter τ. We note that different load–displacement curves are obtained for different loading program parameters τ. Increasing values of the loading program parameter τ correspond to loading processes in which the loadings are applied with increasing prescribed loading rates. For increasing values of τ, the curves of the load-displacement plot rise. This behavior agrees with the experimental evidences in which the inelastic threshold of materials is increased when the loadings are applied with increasing rate, see, e.g., Skrzypek and Hetnarski (1993).

The effect of hardening for the rate-independent material behavior ($\tau = 0$) is described in Fig. 2. In Fig. 2 (top), the maximum equivalent plastic strain exhibited in the solid during the loading process is plotted as a function of the applied load for the elastoplastic material behavior with and without hardening. Herein the load is the sum of the nodal reactions on the bounded upper edge. In Fig. 2 (bottom), the maximum equivalent plastic strain exhibited in the solid is plotted as a function of the prescribed upper edge displacement for the rate-independent elastoplastic material behavior with and without hardening.

The evolution of the plastic strain for increasing prescribed upper edge displacements is illustrated in Fig. 3 for a rate-independent elastoplastic material behavior (corresponding to a loading program parameter $\tau = 0$) without hardening.

For a rate-independent elastoplastic material behavior ($\tau = 0$) with hardening the evolution of the plastic strain is reported in Fig. 4 for increasing prescribed upper edge displacements.
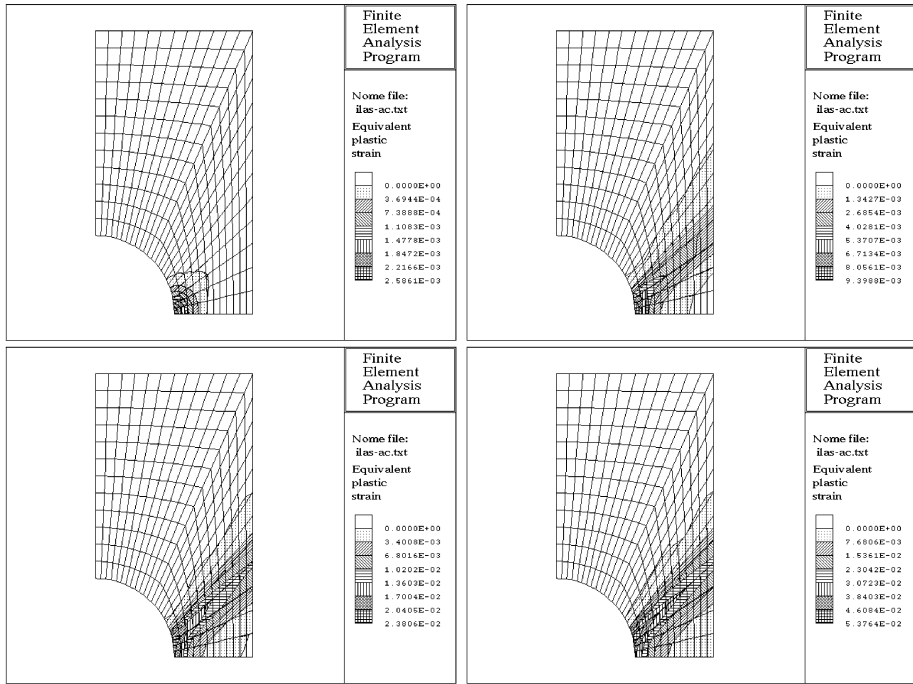
Fig. 3 Rate-independent plasticity without hardening (loading program parameter $\tau = 0$). Evolution of equivalent plastic strains for increasing prescribed upper edge displacements $u = 1.5$ cm (*top left*), $u = 2.5$ cm (*top right*), $u = 5$ cm (*bottom left*), $u = 10$ cm (*bottom right*)

By increasing the loading, we observe that the plastic strains originated at the rim of the hole gradually evolve towards the lateral edge of the perforated strip. The numerical results and the contour plots illustrated in Figs. 3–4 are in agreement with the experimental results analyzed by Theocaris and Marketos (1964). In this regard, see, e.g., Fig. 12 reported by Theocaris and Marketos (1964) on page 388. The agreement with the experimental results confirms the reliability of the numerical simulation analysis for the adopted constitutive relations.

In Fig. 5 (top figures), the evolution of the plastic strain in the strip is shown for rate-independent plasticity ($\tau = 0$) with hardening, by illustrating the contour plots of the equivalent plastic strain for prescribed upper edge displacements respectively set equal to $u = 1.5$ cm (top left) and $u = 2.0$ cm (top right).

For rate-dependent plasticity with hardening, by assuming an increased prescribed loading rate corresponding to a loading program parameter $\tau = 0.2$, the contour plots of the equivalent plastic strain are reported in Fig. 5 (bottom figures) for the prescribed upper edge displacements set equal to $u = 1.5$ cm (bottom left) and $u = 2.0$ cm (bottom right).

The effects of the loading rate on the material response are clearly illustrated in Fig. 6, where the contour plots of the equivalent plastic strains are reported for the same prescribed upper edge displacement ($u = 2.0$ cm) and for different prescribed loading rates corresponding respectively to $\tau = 0$ (Fig. 6 (left)) and $\tau = 0.2$ (Fig. 6 (right)).

When the loading process is applied with an increased prescribed loading rate, in order to investigate the effects of increasing loading rates on the distribution of plastic strains for an elastoplastic material behavior, in Fig. 7 we illustrate the contour plots of the final equivalent
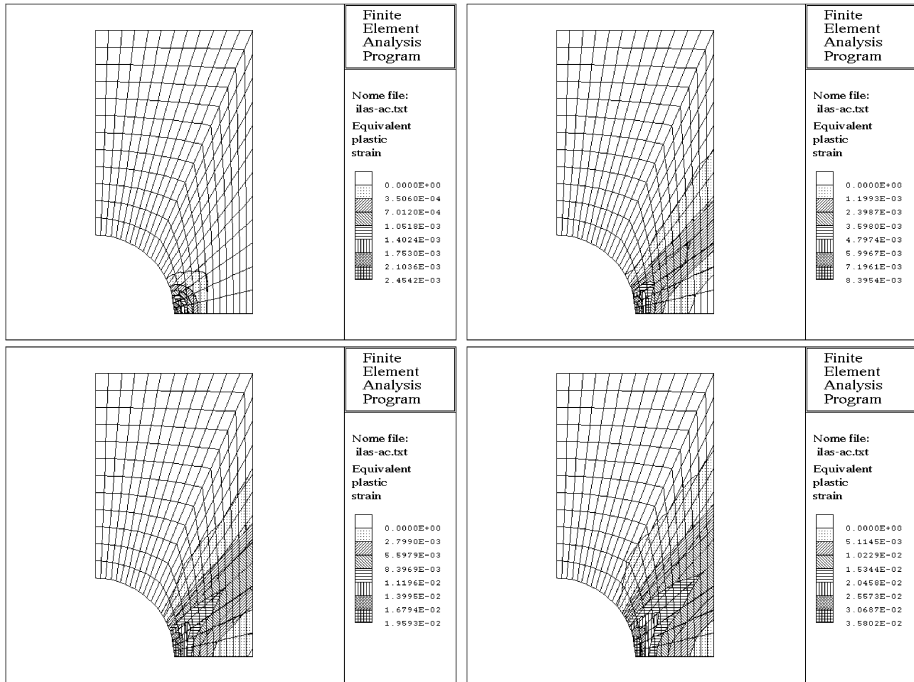
Fig. 4 Rate-independent plasticity with hardening (loading program parameter $\tau = 0$). Evolution of equivalent plastic strain for increasing prescribed upper edge displacements $u = 1.5$ cm (*top left*), $u = 2.5$ cm (*top right*), $u = 5$ cm (*bottom left*), $u = 10$ cm (*bottom right*)

plastic strain corresponding to the final prescribed upper edge displacement $u_{max} = 10$ cm. In Fig. 7, the contour plots of the final equivalent plastic strains are respectively reported for an elastoplastic material behavior *without hardening* by prescribing increasing loading rates corresponding to the loading program parameters $\tau = 0.1, 1, 3$, and 6.

Furthermore, in Fig. 8 in order to analyze the influence of increased loading rates on the plastic material behavior *with hardening*, the contour plots of the equivalent plastic strains are illustrated for the final prescribed upper edge displacement $u_{max} = 10$ cm and for different increased loading rates corresponding to the loading program parameters $\tau = 0.1, 1, 3$, and 6.

When the loadings are applied with an increased prescribed loading rate, the effects of the loading rate on the elastoplastic behavior are described in Fig. 9 where for rate-dependent plasticity the maximum value of the equivalent plastic strain is plotted as a function of the prescribed upper edge displacement for different values of the loading program parameter τ. In the plot it is shown that for a fixed value of the maximum equivalent plastic strain the load increases for increasing values of the loading program parameter τ. For a fixed value of the prescribed upper edge displacement, the maximum equivalent plastic strain decreases for increasing values of the loading program parameter τ.

In Fig. 10, for rate-dependent plasticity without hardening (Fig. 10, top) and rate-dependent plasticity with hardening (Fig. 10, bottom), we illustrate the maximum equivalent plastic strain exhibited in the solid as a function of the applied load and for different prescribed loading rates which are obtained by assigning increasing values of the loading program parameter τ.
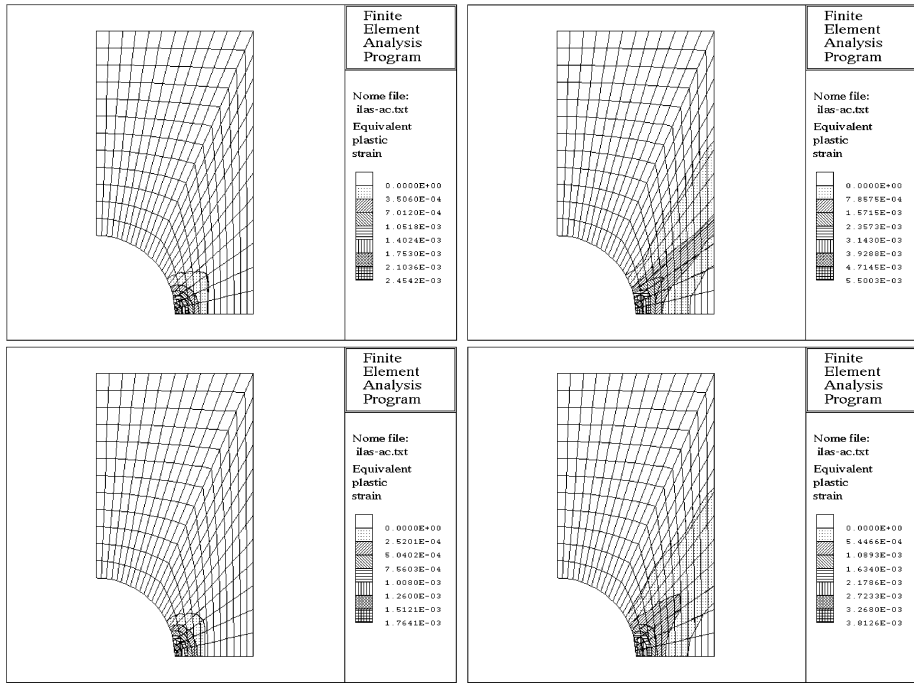
Fig. 5 *Top figures*: Rate-independent plasticity with hardening ($\tau = 0$). Evolution of equivalent plastic strain for the prescribed upper edge displacements $u = 1.5$ cm (*top left*) and $u = 2.0$ cm (*top right*). *Bottom figures*: Rate-dependent plasticity with hardening ($\tau = 0.2$). Evolution of equivalent plastic strain for the prescribed upper edge displacements $u = 1.5$ cm (*bottom left*) and $u = 2.0$ cm (*bottom right*)
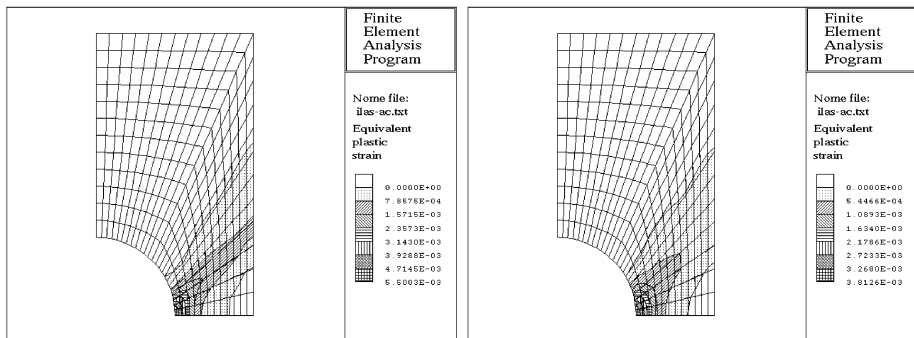

Fig. 6 Rate plasticity with hardening. Contour plots of equivalent plastic strain for the same prescribed upper edge displacement $u = 2.0$ cm and different loading rates corresponding to loading program parameters $\tau = 0$ (*left*) and $\tau = 0.2$ (*right*)

We notice from Fig. 10 that the maximum *final* equivalent plastic strain decreases when the load is applied with increased values of the prescribed loading rate that is with increased values of the loading program parameter τ. Herein the final prescribed displacement corresponds to $u_{\max} = 10$ cm.
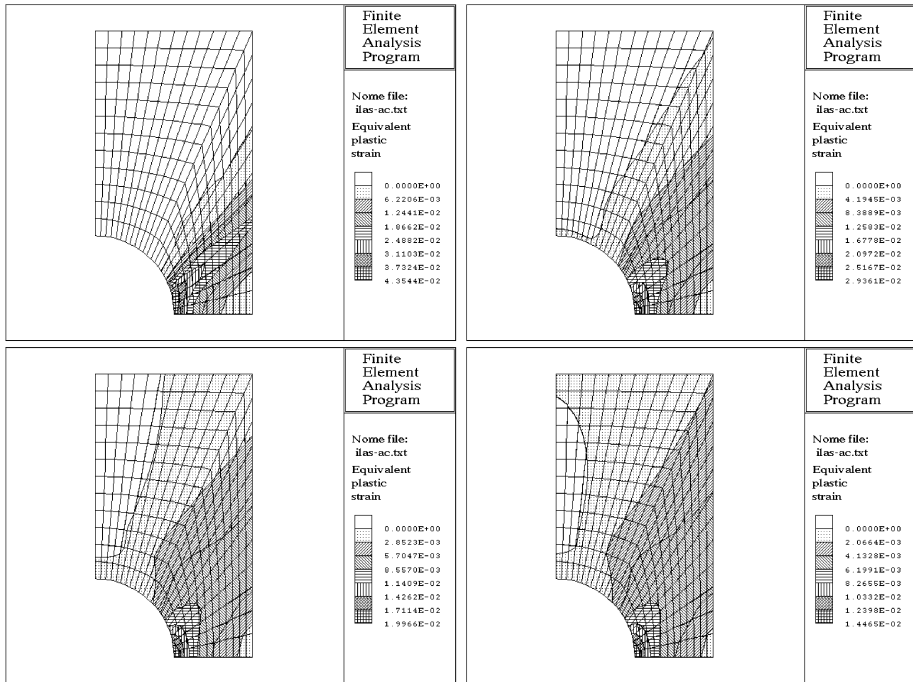
Fig. 7 Rate-dependent plasticity without hardening. Contour plots of the equivalent plastic strain for the final prescribed upper edge displacement ($u_{max} = 10$ cm) and different loading rates corresponding to loading program parameters $\tau = 0.1$ (*top left*), $\tau = 1$ (*top right*), $\tau = 3$ (*bottom left*), $\tau = 6$ (*bottom right*)

In order to better clarify the different influence that hardening has in elastoplasticity when the loading is applied with a null or a prescribed loading rate, we illustrate in Fig. 11 (top left) the contour plot of the final equivalent plastic strain in the solid for rate-independent plasticity ($\tau = 0$) *without hardening* and in Fig. 11 (top right) the contour plot of the final equivalent plastic strain in the solid for rate-independent plasticity ($\tau = 0$) *with hardening*. The different distribution of the plastic strains in the solid is clearly shown for both the contour plot and the magnitude of the plastic strains by comparing Fig. 11 (top left), without hardening, and Fig. 11 (top right) with hardening.

Conversely, when the loading is applied by assigning a considerable high value of the prescribed loading rate ($\tau = 10$), the contour plots of the final equivalent plastic strains in the solid are illustrated in Fig. 11 (bottom left) for rate-dependent plasticity *without hardening* and in Fig. 11 (bottom right) for rate-dependent plasticity *with hardening*.

For plasticity *without hardening*, by comparing Fig. 11 (top left), with null loading rate, and Fig. 11 (bottom left), with a prescribed loading rate $\tau = 10$, we note that by increasing the prescribed loading rate the plastic strains are more distributed in the solid with the result that the final maximum equivalent plastic strain decreases. The same effect of a more diffuse distribution of plastic strains in the solid due to increased prescribed loading rates can also be noticed for plasticity *with hardening*, by comparing Fig. 11 (top right) and Fig. 11 (bottom right).

In Fig. 12 (top), we report the maximum final equivalent plastic strain as a function of the loading program parameter τ for rate-dependent plasticity without hardening. As a matter of
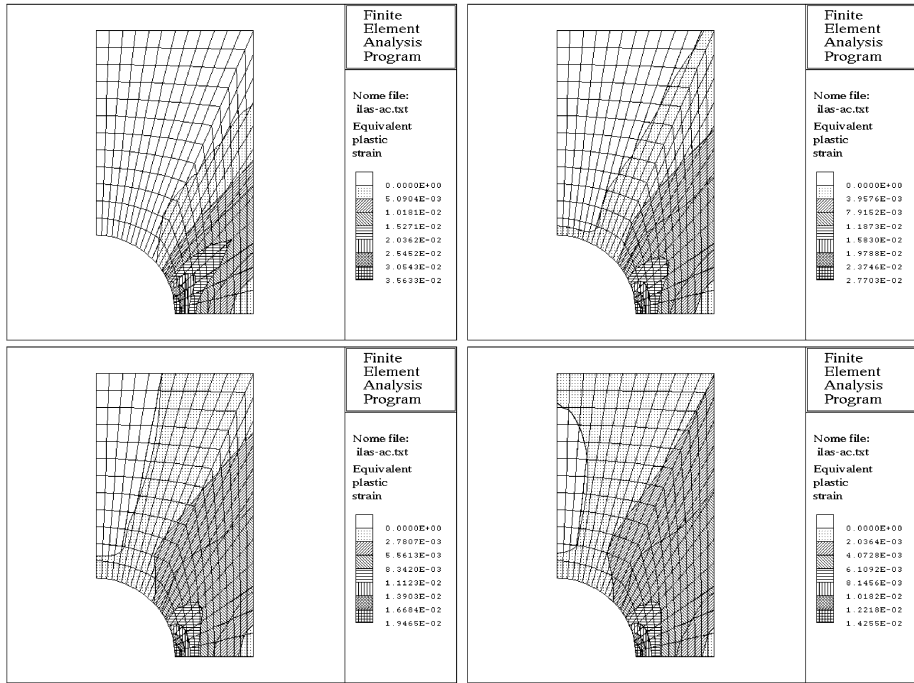
Fig. 8 Rate-dependent plasticity with hardening. Contour plots of the equivalent plastic strain for the final prescribed edge displacement ($u_{max} = 10$ cm) and different loading rates corresponding to loading program parameters $\tau = 0.1$ (*top left*), $\tau = 1$ (*top right*), $\tau = 3$ (*bottom left*), $\tau = 6$ (*bottom right*)


Fig. 9 Maximum equivalent plastic strain vs the imposed upper edge displacement for different loading rates corresponding to increasing loading program parameters τ. Rate-dependent plasticity without hardening
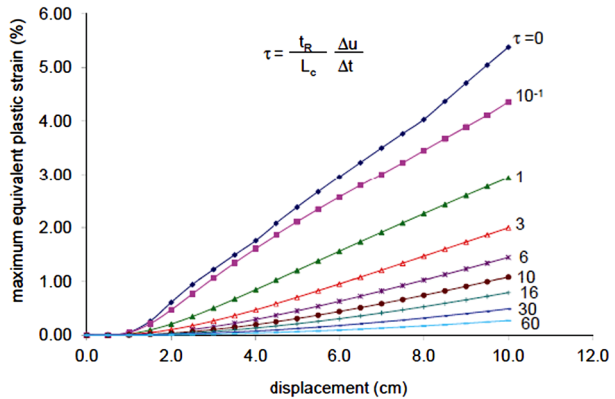
fact, Fig. 12 (top) clearly shows the decrease of the maximum final equivalent plastic strain for increasing values of the prescribed loading rates.

By comparing Fig. 11 (bottom left) and Fig. 11 (bottom right), we observe that for considerably high values of the prescribed loading rate ($\tau = 10$) the extent of the contour plot of the plastic strains for the material without hardening resembles the one for the material with hardening. The same considerations apply with regard to the maximum equivalent plastic strains exhibited in the solid, see Fig. 11 (bottom left) and Fig. 11 (bottom right). These

Fig. 10 Maximum equivalent plastic strain vs applied load for different loading rates corresponding to increasing loading program parameters τ. Rate-dependent plasticity without hardening (*top*) and rate-dependent plasticity with hardening (*bottom*)
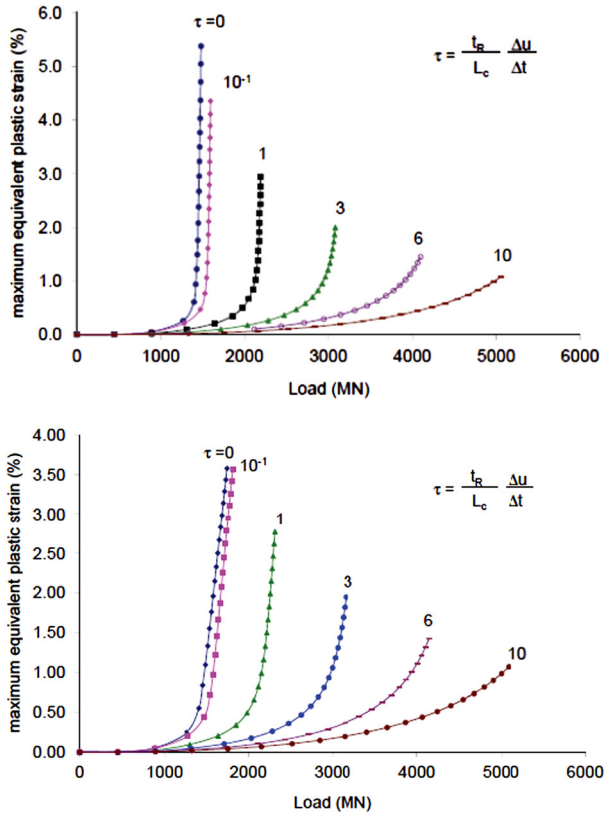
similarities between the plastic behavior without hardening and that with hardening occur for increased values of the prescribed loading program parameter τ, that is, for highly increased values of the loading rate. Conversely, hardening plays a more relevant role on the different distribution of the plastic strains when the loadings are applied with a null loading rate ($\tau = 0$), that is, by comparing Fig. 11 (top left) for plasticity without hardening and Fig. 11 (top right) for plasticity with hardening.

For a further clarification of these aspects, in Fig. 12 (bottom) a comparative analysis of the effects of hardening for increasing prescribed loading rates is illustrated in rate-dependent plasticity. In Fig. 12 (bottom) the maximum final equivalent plastic strain in the solid is plotted as a function of the loading program parameter τ, which describes the influence of the prescribed loading rate of the applied loadings, thus accounting for gradually increasing loading rates. In Fig. 12 (bottom), we note that for increased prescribed loading rates, that is, by assigning increased values of τ, the difference between the maximum final equivalent plastic strain for elastoplasticity without hardening and that with hardening is gradually decreasing.

For increasing values of the prescribed loading rate, that is, for increasing values of τ, the effect of hardening on the maximum equivalent plastic strain is reduced. In fact, from Fig. 12 (bottom) we note that for increased values of the loading program parameter τ the difference is reduced between the two curves representing the maximum final equivalent plastic strain in the elastoplastic material *with hardening* and *without hardening*.
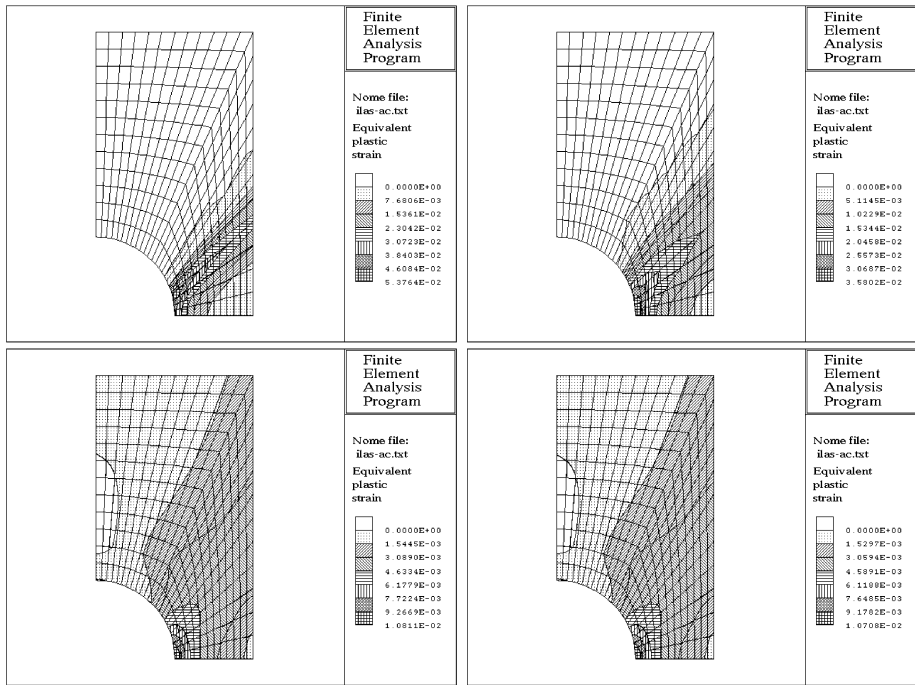
Fig. 11 Contour plot of equivalent plastic strain corresponding to the final prescribed upper edge displacement $u_{max} = 10$ cm. *Top figures*: Rate-independent plasticity ($\tau = 0$). Rate-independent plasticity without hardening (*top left*) and rate-independent plasticity with hardening (*top right*). *Bottom figures*: Rate-dependent plasticity with a considerable high value of the prescribed loading rate ($\tau = 10$). Rate-dependent plasticity without hardening (*bottom left*) and rate-dependent plasticity with hardening (*bottom right*)

6 Conclusions

In this work a suitable finite element solution procedure has been adopted for rate-dependent problems in elastoplasticity, and an implicit algorithmic scheme has been illustrated and implemented into a finite element code. For the simulation of rate-dependent elastoplastic strain-hardening problems, a numerical procedure has been described, which accounts for the effects of the loading rate dependence. An analysis has been detailed on the influence that hardening rules have on the mechanical response of elasto/viscoplastic materials when they are subject to loadings applied with increased prescribed loading rates.

The effects of different loading rates have been investigated for elasto/viscoplastic strain-hardening problems, and the mechanical response of the adopted constitutive material behavior has been analyzed. Hardening rules have a different influence on the mechanical response of materials and structures depending on the different imposition of the loading rate. A comparative analysis has been presented on the effects of hardening in rate-dependent elastoplasticity when the loadings are applied with different prescribed loading rates so that the different influence of hardening is illustrated in the rate-sensitive analysis of elasto/viscoplastic strain-hardening materials and structures.

Numerical applications and computational results have been presented in order to illustrate the influence that hardening rules have in the rate-dependent elastoplastic analysis of structures when the loadings are applied with a null or with increased loading rates. A nu-

Fig. 12 Maximum final equivalent plastic strain exhibited in the solid vs the loading program parameter τ: (*top*) rate-dependent plasticity without hardening; (*bottom*) comparative analysis between rate-dependent plasticity without hardening (*upper curve*) and rate-dependent plasticity with hardening (*lower curve*)
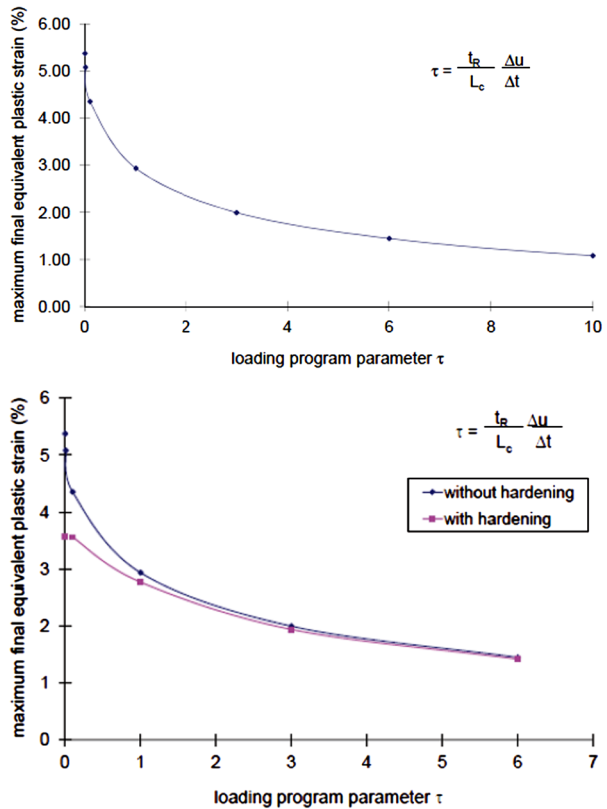
merical simulation has been presented of the influence due to hardening on the plastic strains in the rate-dependent elastoplastic analysis of structures subject to different rate-dependent loading programs.

Computational applications have been illustrated by showing numerically that hardening has a reduced influence on the amplitude of the maximum equivalent plastic strains when the loadings are applied with an increased prescribed loading rates with respect to the case without hardening. Accordingly, for elasto/viscoplastic strain-hardening materials and structures when the loadings are applied with increased prescribed loading rates the influence of hardening has a gradually reduced effect on the amount and distribution of the maximum equivalent plastic strains with respect to the elasto/viscoplastic material behavior without hardening.

References

Abed, F.: Constitutive modeling of the mechanical behavior of high strength ferritic steels for static and dynamic applications. Mech. Time-Depend. Mater. **14**, 329–345 (2010)

Armstrong, P., Frederick, C.: A mathematical representation of the multiaxial Baushinger effect. Technical report RD/B/N731, Central Electricity Generating Board, Berkeley, UK (1966)

Artioli, E., Auricchio, F., da Veiga, L.B.: Second-order accurate integration algorithms for the von Mises plasticity with a nonlinear kinematic hardening mechanism. Comput. Methods Appl. Mech. Eng. **196**, 1827–1846 (2007)

Autenrieth, H., Schulza, V., Herzig, N., Meyer, L.: Ductile failure model for the description of AISI 1045 behavior under different loading conditions. Mech. Time-Depend. Mater. **13**, 215–231 (2009)

Brnic, J., Turkalj, G., Canadija, M., Lanc, D., Krscanski, S.: Martensitic stainless steel AISI 420—mechanical properties, creep and fracture toughness. Mech. Time-Depend. Mater. **15**, 341–352 (2011)

Chaboche, J.: A review of some plasticity and viscoplasticity constitutive theories. Int. J. Plast. **24**, 1642–1693 (2008)

D'Amore, A., Grassia, L.: Constitutive law describing the strength degradation kinetics of fibre-reinforced composites subjected to cyclic loading. Mech. Time-Depend. Mater. **20**(1), 1–12 (2016)

D'Amore, A., Grassia, L., Verde, P.: Modeling the flexural fatigue behavior of glass-fiber-reinforced thermo-plastic matrices. Mech. Time-Depend. Mater. **17**(1), 15–23 (2013)

DeAngelis, F.: An internal variable variational formulation of viscoplasticity. Comput. Methods Appl. Mech. Eng. **190**, 35–54 (2000)

DeAngelis, F.: A comparative analysis of linear and nonlinear kinematic hardening rules in computational elastoplasticity. Tech. Mech. **32**(2–5), 164–173 (2012)

DeAngelis, F.: Computational issues and numerical applications in rate-dependent plasticity. Adv. Sci. Lett. **19**(8), 2359–2362 (2013)

DeAngelis, F., Cancellara, D.: Multifield variational principles and computational aspects in rate plasticity. Comput. Struct. **180**, 27–39 (2017)

DeAngelis, F., Taylor, R.: An efficient return mapping algorithm for elastoplasticity with exact closed form solution of the local constitutive model. Eng. Comput. **32**(8), 2259–2291 (2015)

DeAngelis, F., Taylor, R.: A nonlinear finite element plasticity formulation without matrix inversions. Finite Elem. Anal. Des. **112**, 11–25 (2016)

Duvaut, G., Lions, J.: Les Inequations en Mécanique et en Physique. Dunot, Paris (1992)

Farrahi, G., Ghodrati, M., Azadi, M., Rad, M.R.: Stress–strain time-dependent behavior of a 356.0 aluminium alloy subjected to cyclic thermal and mechanical loadings. Mech. Time-Depend. Mater. **18**, 475–491 (2014)

Halphen, B., Nguyen, Q.: Sur les matériaux standards généralisés. J. Méc. **14**, 39–63 (1975)

Hill, R.: The Mathematical Theory of Plasticity. Clarendon Press, Oxford (1950)

Hiriart-Urruty, J., Lemarechal, C.: Convex Analysis and Minimization Algorithms, vols. I–II. Springer, Berlin (1993)

Ishlinsky, A.J.: General theory of plasticity with linear strain hardening. Ukr. Mat. Zh. **6**, 314 (1954)

Lemaitre, J., Chaboche, J.: Mechanics of Solids Materials. Cambridge University Press, Cambridge (1990)

Luenberger, D.: Introduction to Linear and Non-Linear Programming. Addison-Wesley, Reading (1973)

Marotti de Sciarra, F.: Nonlocal and gradient rate plasticity. Int. J. Solids Struct. **41**, 7329–7349 (2004)

Marotti de Sciarra, F.: Variational formulations, convergence and stability properties in nonlocal elastoplasticity. Int. J. Solids Struct. **45**, 2322–2354 (2008)

Naghdi, P., Murch, S.: On the mechanical behaviour of viscoelastic/plastic solids. J. Appl. Mech. **30**, 321–328 (1963)

Perzyna, P.: The constitutive equations for rate sensitive materials. Q. Appl. Math. **20**, 321–332 (1963)

Perzyna, P.: Fundamental problems in viscoplasticity. In: Advances in Applied Mechanics, vol. 9, pp. 243–377. Academic Press, San Diego (1966)

Pina, J., Kouznetsova, V., Geers, M.: Elevated temperature creep of pearlitic steels: an experimental-numerical approach. Mech. Time-Depend. Mater. **18**, 611–631 (2014)

Prager, W.: A new method of analyzing stresses and strains on work-hardening plastic solids. ASME J. Appl. Mech. **23**, 493–496 (1956)

Simo, J.: Numerical analysis and simulation of plasticity. In: Ciarlet, P., Lions, J. (eds.) Handbook of Numerical Analysis, vol. VI. Elsevier, Amsterdam (1998)

Simo, J., Hughes, T.: Computational Inelasticity. Springer, New York (1998)

Simo, J., Kennedy, J., Govindjee, S.: Non-smooth multisurface plasticity and viscoplasticity. Loading/unloading conditions and numerical algorithms. Int. J. Numer. Methods Biomed. Eng. **26**, 2161–2185 (1988)

Skrzypek, J., Hetnarski, R.: Plasticity and Creep. CRC Press, Boca Raton (1993)

Theocaris, P., Marketos, E.: Elastic-plastic analysis of perforated thin strips of a strain-hardening material. J. Mech. Phys. Solids **12**, 377–390 (1964)

Valoroso, N., Rosati, L.: Consistent derivation of the constitutive algorithm for plane stress isotropic plasticity. Part I: Theoretical formulation. Int. J. Solids Struct. **46**, 74–91 (2009a)

Valoroso, N., Rosati, L.: Consistent derivation of the constitutive algorithm for plane stress isotropic plasticity. Part II: Computational issues. Int. J. Solids Struct. **46**, 92–124 (2009b)

Yosida, K.: Functional Analysis, vols. I–II, 6th edn. Springer, Berlin (1980)

Zienkiewicz, O., Taylor, R., Fox, D.: The Finite Element Method for Solid and Structural Mechanics, 7th edn. Elsevier, Oxford (2013)